Supplemental Materials

Molecular Biology of the Cell

Buxboim et al.

Supplementary figure legends

Figure S1: **Myosin-IIA is essential for cell & nucleus mechanosensitivity of matrix stiffness**

(A) Representative images of MSCs spreading more on stiff gels and less on soft gels after 36 hours in culture but not if treated with Blebb myosin-II inhibitor. Scale-bar: 40 μm. (B) Projected areas of (i) cells and (ii) nuclei increase monotonically with matrix stiffness but Blebb-treated cells show no matrix-dependence. Both cellular and nuclear spreading areas of MSCs satisfy hyperbolic fits with half spreading response elasticity E_0 = 3.3 kPa. (C) Immunofluorescence images of MSCs expanded on plastic for 2-8 weeks are shown here at passage P2, P4 and P7 after 36 hours of culture on gels. Scale-bar: 20 μm. (D) While maintaining a linear correlation between nucleus and cell projected areas, the canonical spreading hierarchy *soft* < *thin* < *stiff* is satisfied predominantly at early passage whereas P7 cells altogether exhibit larger spreading areas than early passage cells. Inset: the ratio between cells projected areas that are obtained for soft versus stiff gels reflects the extent of cellular mechanosensitivity to matrix stiffness. Soft-to-stiff spreading ratio of late passage cells is close to 1, yet P2 cells spread three-fold more on stiff gels compared to soft. (E) Cellular mechano-sensivity and senescence: MSCs were expanded in culture for 8 weeks (standard plastic flasks) during which cells underwent 7 passages (P7). To interrogate cellular mechanosensitivity, MSCs were trypsin-detached at passage P2, P4 and P7, cultured for 36 hours on soft (1 kPa), soft and thin (2-3 μm, apparent μ-elasticity 6 kPa) and stiff (40 kPa) gels and lamin-A,C levels were evaluated by quantitative immunofluorescence (qIF). Low passage P2 MSCs show maximal mechanosensitivity, as exemplified relative to the passage-mean trend (black), which diminishes with increasing passage.

Figure S2: **Cell spreading & nucleus flattening dynamics during matrix engagement and adhesion**

(A) Following seeding, the dynamics of cell spreading and nucleus stretching during adhesion to glass surfaces satisfies a hyperbolic fit, with $t_{1/2}$ = 45 min half time both for cell and nucleus projected areas. (A-ii) The cell-to-nucleus projected area ratio dynamics also obeys a $t_{1/2}$ = 45 min hyperbolic fit. As cells spread, cell-to-nucleus projected area increases from 3.3 to 16. Non-adherent cells correspond to t→0 limit. Under the assumption that cells and nuclei are rounded in suspension, we conclude that nucleus volume is 6 fold smaller than cell volume.

Figure S3: **Fresh MSCs are isolated from human bone marrow donors and cultured within hours**

Bone marrow cells are isolated from fresh aspirates and purified by rinse. Mono-nucleated CD34-depleated cells (see methods) were allowed to settle down for 30 min and engage collagen-coated soft-thin gels (1 kPa, 2-3 μm) followed by 3-4 hours of agitation. To screen for strongly adhesive cells, gel substrates were immersed in PBS and positioned perpendicular to the plane of agitation. Gels were subjected to flow-induced stress for 0-to-20 min. Cells were then re-immersed in medium, incubated for 12 hours and fixed and immunostained. (A) Representative images show a transition from a rounded to a prototypical mesenchymal dendritic morphology with increasing flow time. Scale-bar: 40 μm. (B) (i) Flow-induced stress is shown to remove ~50% of the cells but the prolongation of flow shows no accumulative effect, consistent with the removal of weakly adherent cells already after < 2.5 minutes. The fraction of attached cells is computed relative to the number to seeded cells. (ii-iii) In response to the mechanical stresses that are induced by flow, cell projected area and lamin-A,C levels increase concomitantly with nucleus projected area (cell/nucleus

projected area slope 30) with rinse time. This increase in spreading and in lamin-A,C levels is reminiscent of the transition between 'soft' to 'stiff' cellular phenotypes which is shown above to be induced by matrix stiffness or thinness, and consistent with matrix adhesion and spreading dynamics and molecular and drug perturbations of lamin- A and myosin-II (sketched in Fig. 4A-i). (C) Plastic-adhering colony-forming isolated cells were expanded in standard plastic flasks and interrogated by flow cytometry. Cells express MSC surface markers (CD105, CD166, CD44, CD90) and lack expression of hematopoietic markers (CD34, CD45RA) as calibrated versus secondary antibody controls.

Figure S4: **Validation of lamin-A,C overexpression and knockdown, myosin relaxation and nucleus stiffening**

(A, i) Bimodal distribution confirms lamin-A-GFP transfection of 30% of the cells. (ii) A decrease in GFP intensity and a left shift of the GFP-positive cells distribution is induced by siLMNA knockdown. (B) Immunoblot confirms lamin-A transduction, showing a GFP-conjugated lamin-A band. (C) DNA microarray transcript profiling of blebbistatin-treated versus non-treated MSCs: cell relaxation decreases myosin-IIA and LMNA RNA levels but not LBR. (D) The more GFP-lamin-A is expressed, the stiffer the nucleus becomes as evaluated by micropipette aspiration measurements. The extent of nuclear deformation in A549 lung epithelial cells was evaluated after 180 sec of aspirating nuclei that express GFP-lamin-A over a range of > 10 fold. Fits of the stiffening of the nucleus as a function of the increase in lamin-A levels above the average wild-type level indicates a 0.5 power law.

Figure S5: **Lamin-A,C and Myosin-IIA maintain cytoskeletal-nucleoskeletal feedback**

(A) After just 2 hrs of adhesion and spreading, lamin-A,C and myosin-IIA levels increase in MSCs. Myosin-II inhibition subsequently suppresses both proteins. (B) With cell adhesion and spreading lamin-A,C and myosin-IIA levels both increase by 1-2 hrs unless lamin-A,C is knocked down (KD). Plots show single-cell quantitative immunofluorescence intensities (n ~ 50 cells per condition), with myosin-IIA suppression at 36 hrs confirmed by immunoblot (above) and by Mass Spectrometry (below) averaged over of multiple tryptic peptides (detected in 60-80 kDa range).

Figure S6: **Modulation of Lamin-A and LBR leads to change of LBR per LMNA stoichiometry**

(A) LBR (red) were depleted in A549 cells by the shLBR treatment. (B) Knockdown of Lamin-A by shLMNA leads to an increase in LBR per LMNA stoichiometry, while knockdown of LBR decreases the stoichiometry (n > 200 cells per group).

Figure S7: **Analyses of nuclear shape and volume of MSC's after lamin-A,C knockdown, based on fluorescence intensity of Hoechst-labeled DNA and an assumption of ellipsoidal shapes.**

Figure S8: **Less bone and more fat with low lamin-A,C: MSCs and osteoblasts favor bone resorption by osteoclasts after *LMNA* knockdown, and the transcription factor sterol response binding protein-1 (SREBP1) promotes expression of *LBR* in the lipid biosynthesis pathway.**

(A) MSCs and osteoblasts contribute to bone resorption via osteoclasts (Roux and Orcel 2000, Teti 2013), and lamin-A,C knockdown in MSCs on rigid plastic favors such a process relative to control cells. Osteoclast precursors differentiate in the presence of macrophage colony-stimulating factor, M-CSF: deficient mice develop an osteoperosis that is characterized by the absence of osteoclasts, and local injections of M-CSF in bone increase *in situ* osteoclast differentiation and bone resorption. Osteoprotegerin (*TNFRSF11B*) reduces the production of osteoclasts by inhibiting the differentiation of precursors. *CTHRC1* expression in bone is blunted by aging where bone resorption tends to dominate, and it is stimulated by treatment with soluble RANKL (*TNFSF11*) with an initial phase of bone resorption. Hepatocyte growth factor (*HGF*) signals human osteoblasts to express osteopontin (*SPP1*), with inhibition of the HGF receptor (*MET*) decreasing osteopontin production. A role for the transcription factor vitamin-D receptor (*VDR*), such as in expression of RANKL, is likely given that 1,25-dihydroxyvitamin-D_3 together with parathyroid hormone increase bone resorption, primarily via an indirect mechanism mediated by osteoblasts. Many other genes are involved but most or all do not change as much as the indicated genes after lamin-A,C knockdown in the MSCs.

(B) Screenshot of ENCODE data showing ChIP-Seq results for SREBP1 binding to the promoter region of *LBR* gene.

Supplementary References

Roux S and Orcel P (2000). Bone loss. Factors that regulate osteoclast differentiation: an update. *Arthritis Res* 2(6), 451-456.

Teti A (2013). Mechanisms of osteoclast-dependent bone formation. *Bonekey Rep* 2, 449.

Figure S1

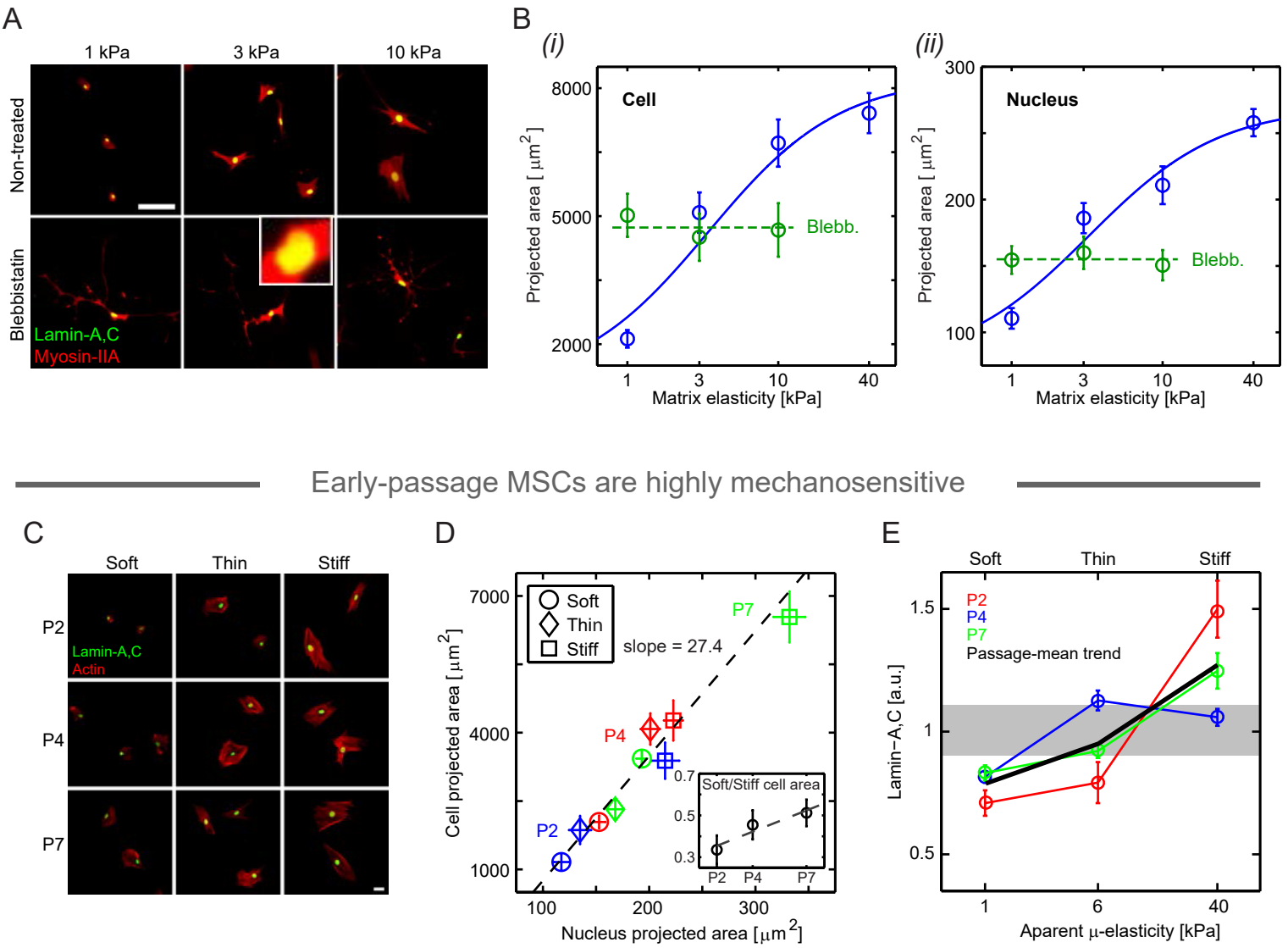
Cell & nuclear morphology of MSCs respond to matrix elasticity unless myosin-II is inhibited
A
1 kPa
3 kPa
10 kPa
Non-treated
Blebbistatin
Lamin-A,C
Myosin-IIA
B
(i)
Cell
Projected area [μm2]
8000
5000
2000
Blebb.
1
3
10
40
Matrix elasticity [kPa]
(ii)
Nucleus
300
200
100
Blebb.
Early-passage MSCs are highly mechanosensitive
C
Soft
Thin
Stiff
P2
P4
P7
Lamin-A,C
Actin
D
Soft
Thin
Stiff
slope = 27.4
Cell projected area [μm2]
7000
4000
1000
100
200
300
Nucleus projected area [μm2]
Soft/Stiff cell area
0.7
0.5
0.3
E
Soft
Thin
Stiff
P2
P4
P7
Passage-mean trend
Lamin−A,C [a.u.]
1.5
1
0.5
1
6
40
Aparent μ-elasticity [kPa]

Figure S2

Cells spread and nuclei flatten within < 1 hr of adhesion

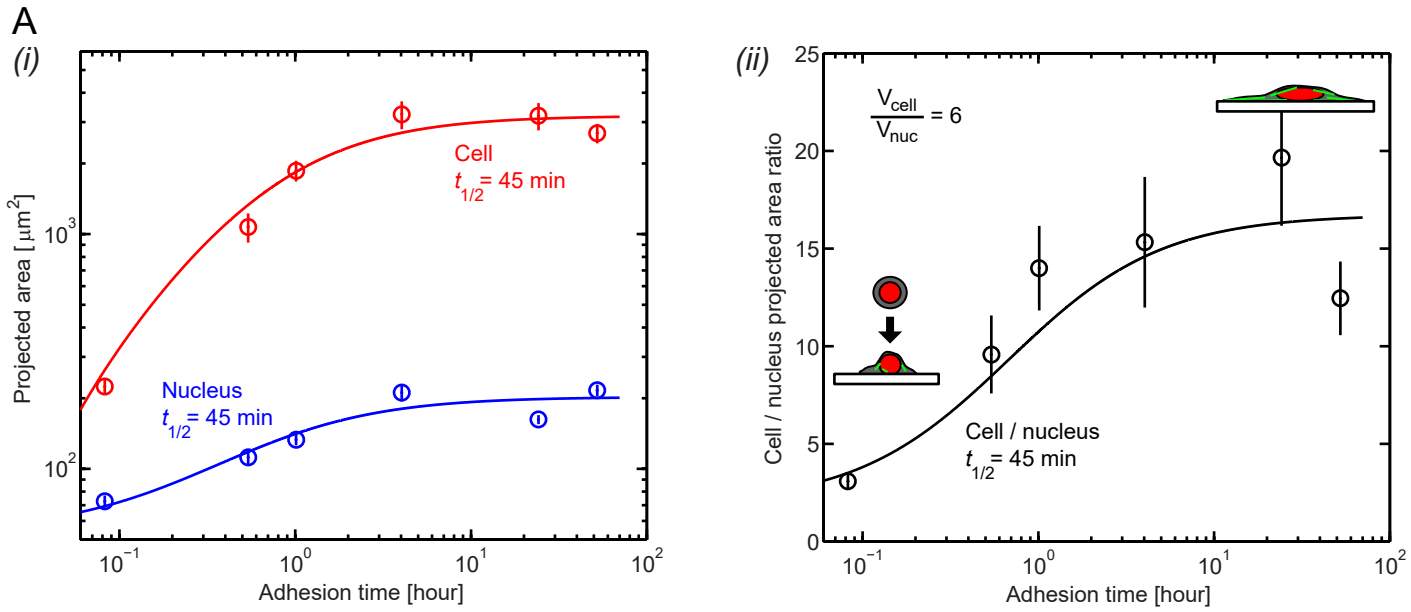

Figure S3

Fresh MSCs are adherent and mechanosensitive

Surface markers confirm MSCs

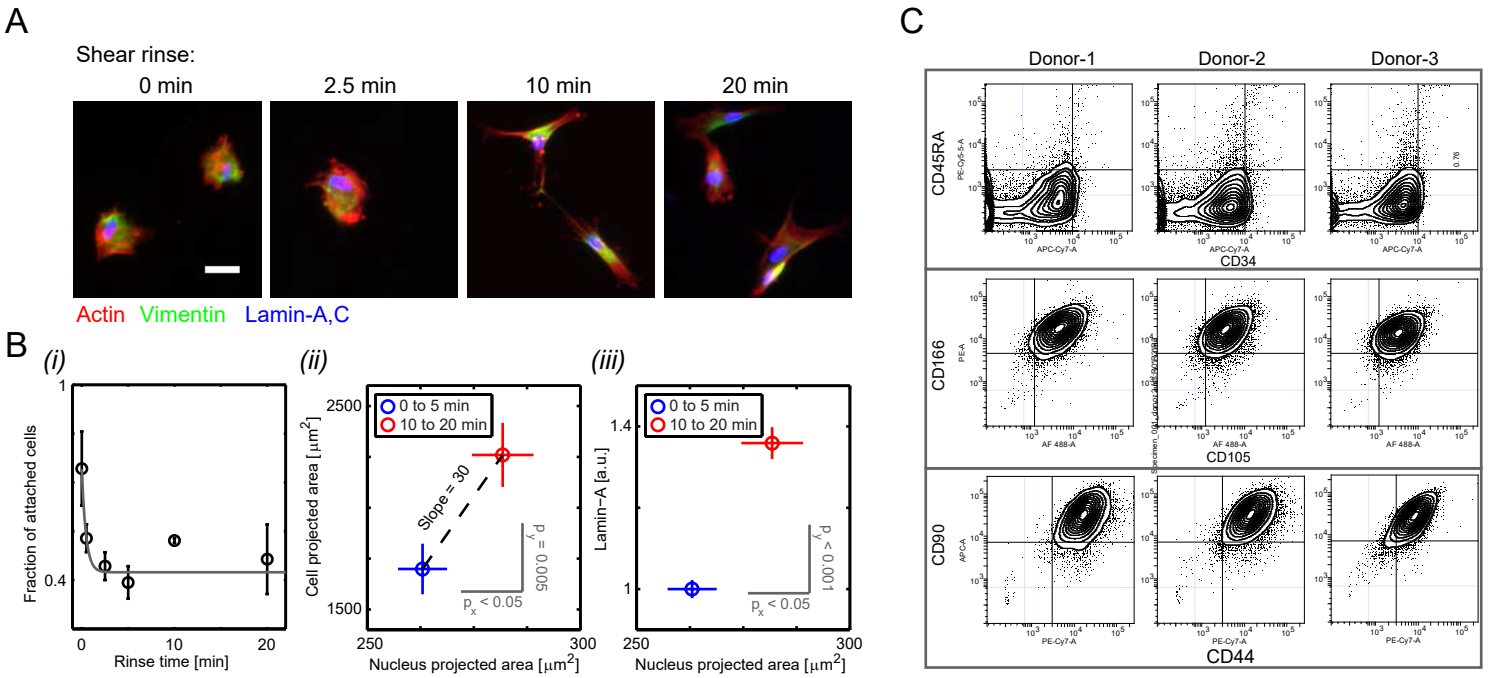

Figure S4

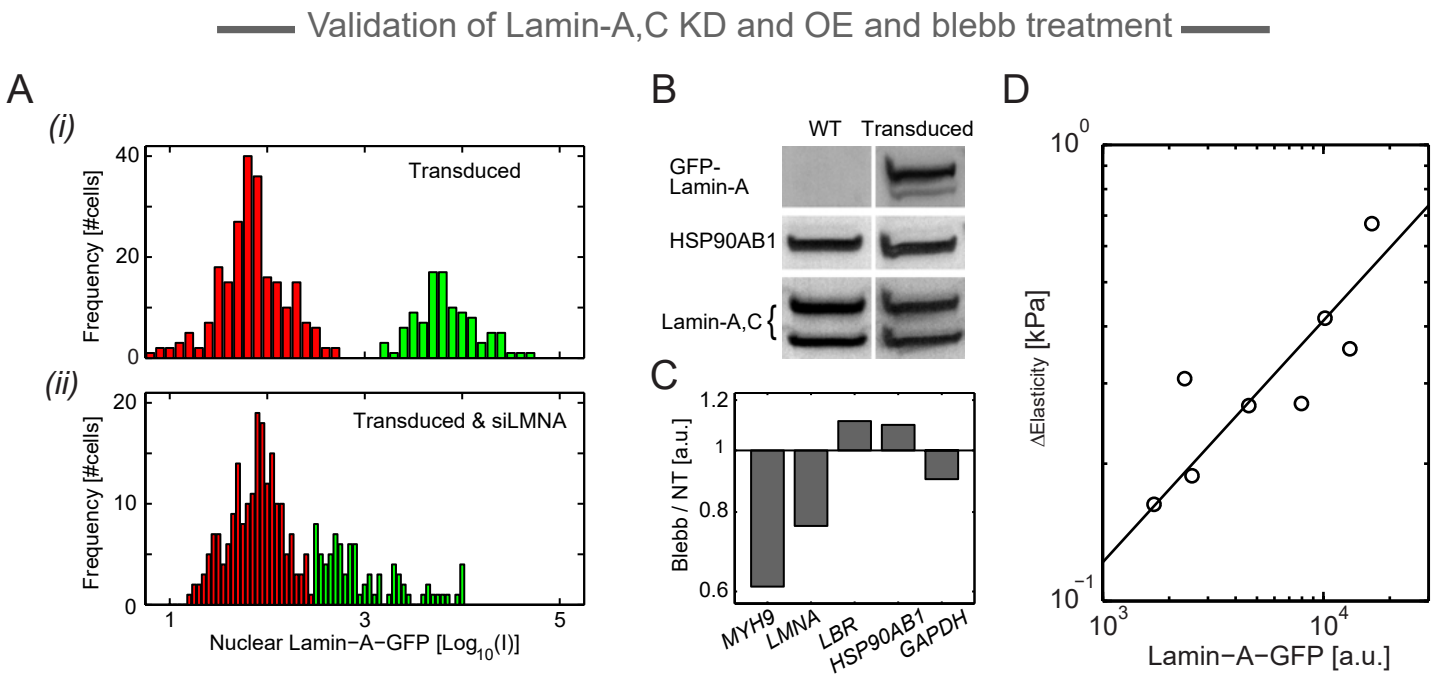
Validation of Lamin-A,C KD and OE and blebb treatment
A
(i)
Transduced
Frequency [#cells]
(ii)
Transduced & siLMNA
Nuclear Lamin−A−GFP [Log10(I)]
B
WT
Transduced
GFP-Lamin-A
HSP90AB1
Lamin-A,C
C
Blebb / NT [a.u.]
MYH9
LMNA
LBR
HSP90AB1
GAPDH
D
ΔElasticity [kPa]
Lamin−A−GFP [a.u.]

Figure S5

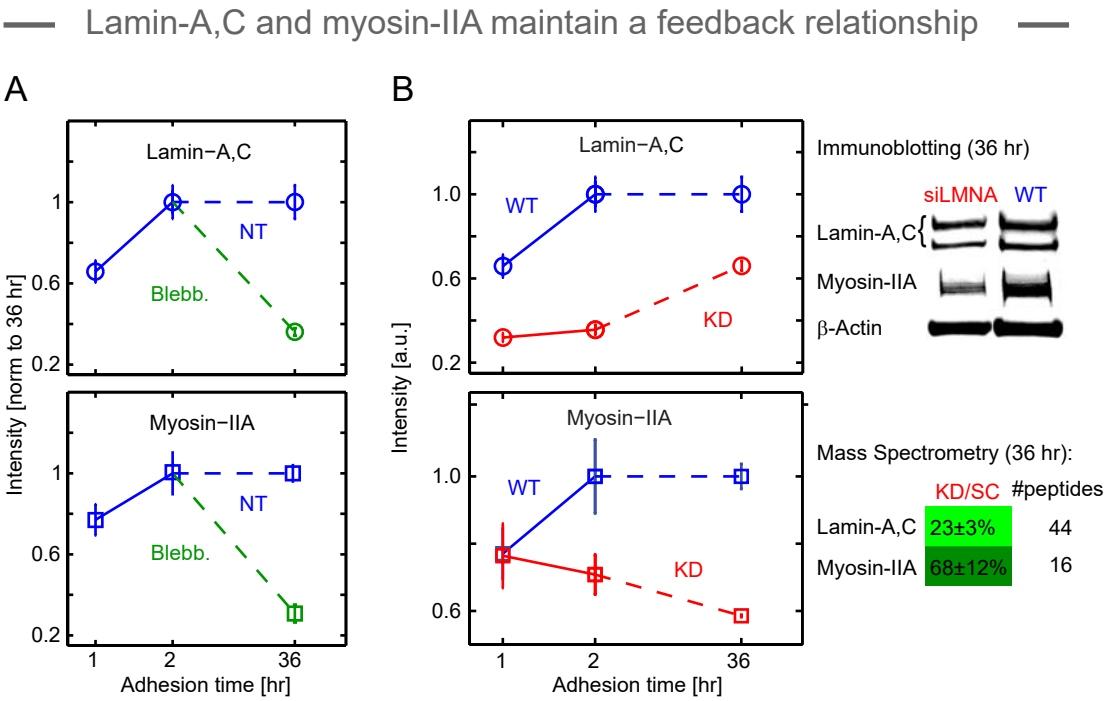
Lamin-A,C and myosin-IIA maintain a feedback relationship
A
Lamin−A,C
Myosin−IIA
NT
Blebb.
Intensity [norm to 36 hr]
1
0.6
0.2
1
2
36
Adhesion time [hr]
B
Lamin−A,C
Myosin−IIA
WT
KD
Intensity [a.u.]
1.0
0.6
1
2
36
Adhesion time [hr]
Immunoblotting (36 hr)
siLMNA
WT
Lamin-A,C
Myosin-IIA
β-Actin
Mass Spectrometry (36 hr):
KD/SC
#peptides
Lamin-A,C
23±3%
44
Myosin-IIA
68±12%
16

Figure S6

Modulation of LBR per LMNA stoichiometry

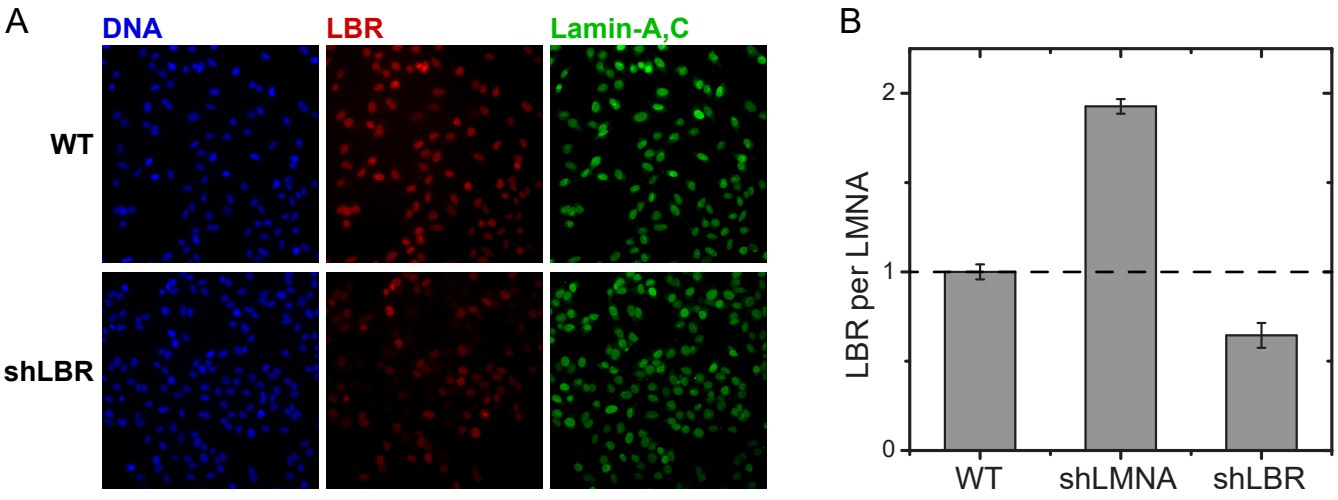

Figure S7

Shape and Intensity analyses: Nuclear Height * [DNA conc] ~ 1 / Area

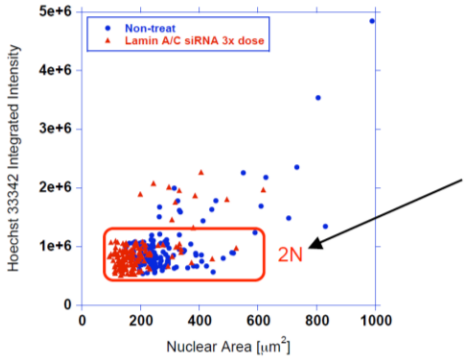

This population used for following plots.

DNA amount ~ constant

but [DNA conc] = DNA / *V*

could vary with variation of

Nuclear Volume *V*

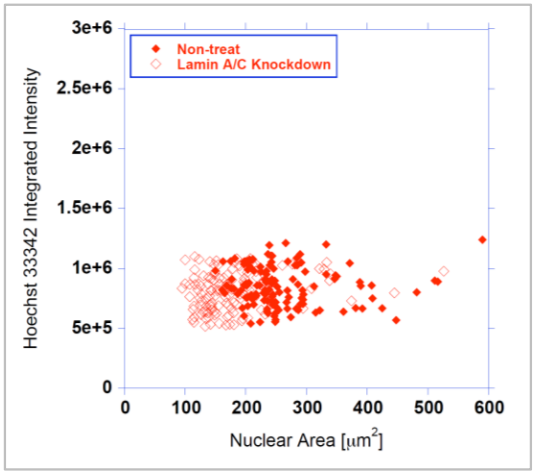

Nuclear Contour Ratio (NCR) = $\frac{4\pi \times (\text{Nuclear Area})}{(\text{Perimeter})^2}$

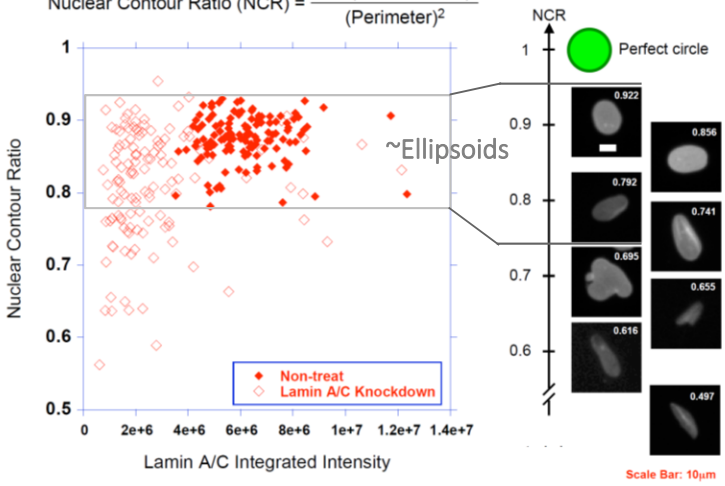

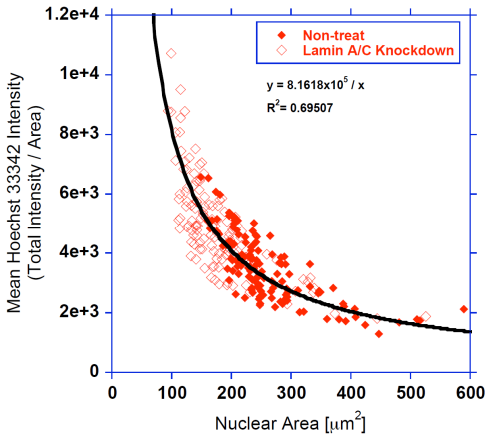

Ellipsoid Approximation:

Volume $V = {}^4/_3\ \pi\ a\ b\ c$

Projected Area $A = \pi\ ab$

Height $H = 2\ c = {}^3/_2\ V / A$

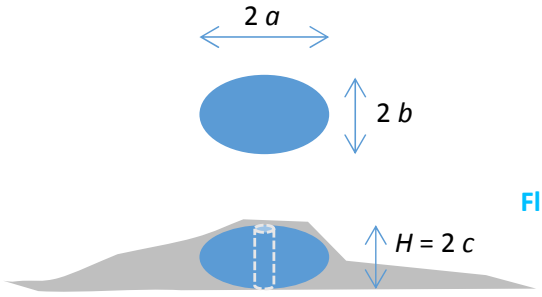

Fluorescence Intensity: $I_{tot} = \phi\ V$ [DNA conc]

$I_{tot} / A = {}^2/_3\ \phi\ H$ [DNA conc]

expt: $I_{tot} / A =$ const / A = const' H [DNA conc]

Fluorescence Intensity:

$I_{center} = \phi\ \alpha\ H$ [DNA conc]

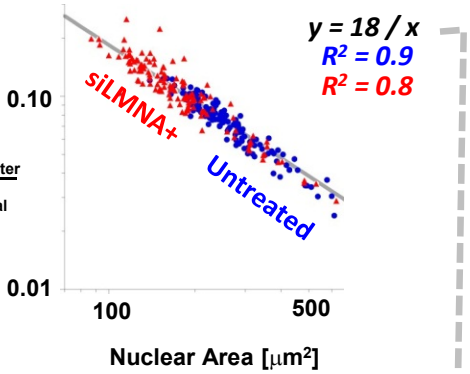

Intensity Test of Ellipsoid Approximation:

expt: $I_{center} / I_{tot} = 18\ \mu m^2 / A$

Fluorescence $H / V = 18\ \mu m^2 / \alpha\ A$

Ellipsoid ${}^3/_2\ / A = ({}^3/_2\ / A)\ (12\ \mu m^2 / \alpha)$

Figure S8

Bone loss is favored by Lamin-A,C knockdown

A

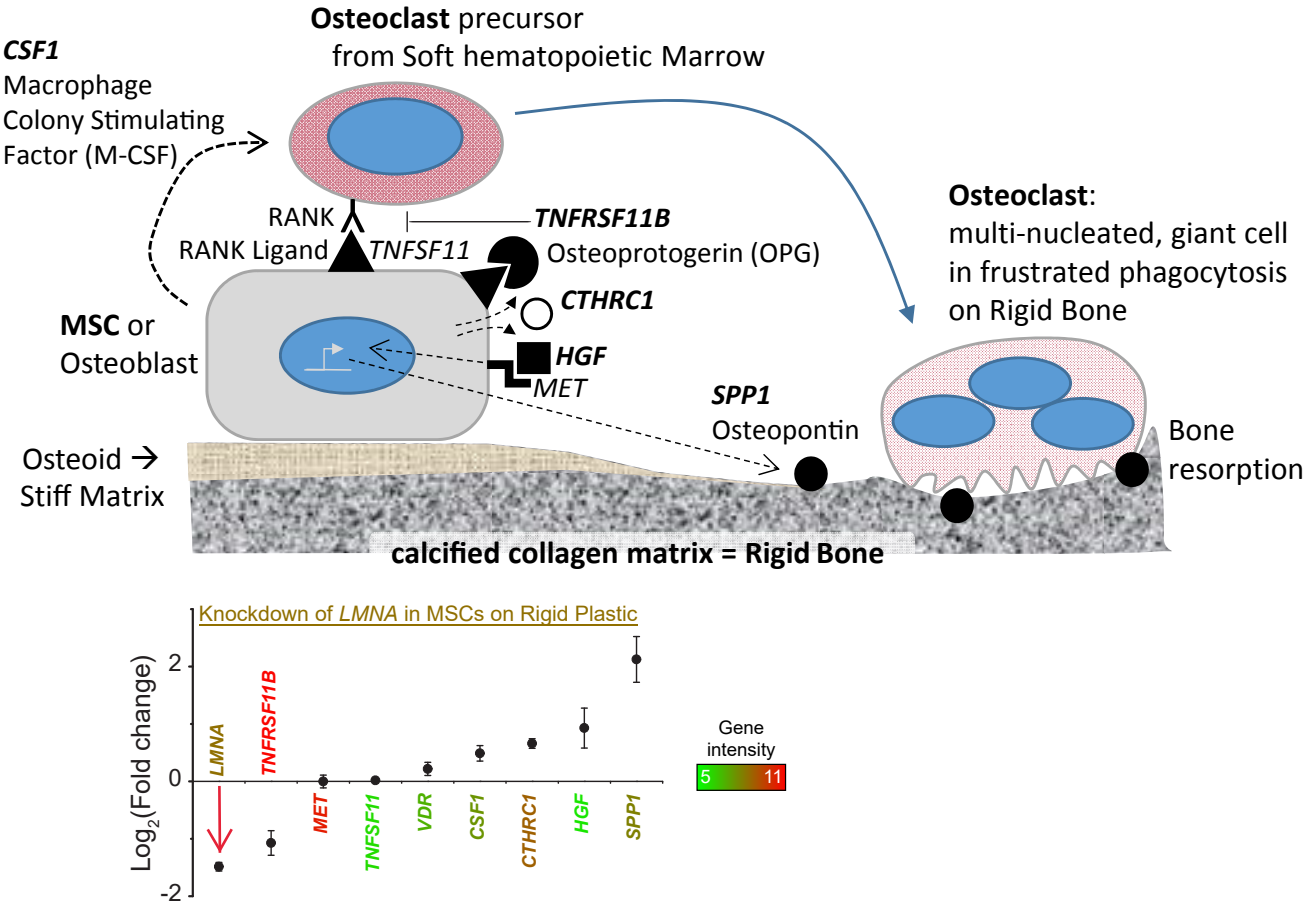

Adipogenic transcription factor SREBP1 regulates expression of sterol reductase *LBR*

B

UCSC genome browser ENCODE database. Screenshot Sept.1, 2017

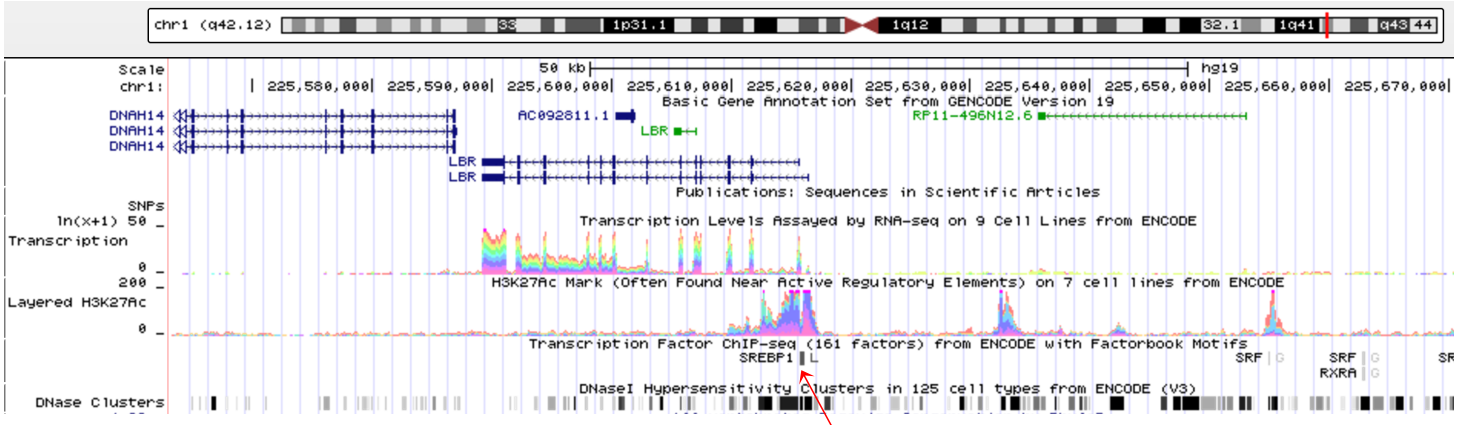

Transcription Factor ChIP-seq (161 factors) from ENCODE with Factorbook Motifs

Factorbook Link: SREBP1
Factor: SREBP1
Cluster Score (out of 1000): 678
Position: chr1:225615747-225616116
Band: 1q42.12
Genomic Size: 370
View DNA for this feature (hg19/Human)

Assays for SREBP1 in Cluster

#	signal	abr	cellType	factor	antibody	treatment	lab	more info
1	678.00	L	HepG2	SREBP1	SREBP1	insulin	Stanford	metadata